

Structure of Active Adlayers on Bimetallic Surfaces: Oxygen Reduction on Au(111) with Bi Adlayers

K. Tamura,^{*,†} B. M. Ocko,[†] J. X. Wang,[‡] and R. R. Adžić[‡]

Department of Physics and Materials Science Department, Brookhaven National Laboratory, Upton, New York 11973-5000

Received: August 1, 2001; In Final Form: January 2, 2002

The structure of Bi adlayers on the Au(111) electrode surface during the course of O₂ reduction has been investigated by in situ surface X-ray scattering. Under oxygen reduction conditions, both the low-coverage (2 × 2)-Bi and the close-packed ($p \times \sqrt{3}$)-2Bi adlayer structures are stable. We developed an electrochemical drop cell that provides a more uniform potential distribution during high current conditions compared with commonly used thin-layer cells. Our results clearly indicate distinctly different catalytic properties for the two ordered bismuth adlayer phases. In the potential region corresponding to the (2 × 2)-Bi phase, O₂ reduction is promoted to a four-electron reaction, albeit with relatively slow kinetics. The close-packed ($p \times \sqrt{3}$)-2Bi phase, formed at more negative potentials, appears to have a limited number of sites available for four-electron reduction, but the reaction kinetics on this adlayer is enhanced by an increased overpotential.

1. Introduction

Electrocatalytic oxygen reduction is of paramount importance for electrochemical energy conversion in fuel cells and metal–air batteries and plays a major role in corrosion processes. It continues to attract considerable attention because of its complex kinetics and the need for better electrocatalysts for more efficient fuel-cell cathodes. Recent efforts to develop improved fuel cells have revived interest in improving electrocatalysts for O₂ reduction.¹ Metal adlayers, formed by underpotential deposition (UPD), can have pronounced catalytic effects on O₂ reduction on Au. They positively shift the half-wave O₂ reduction potential and, in some cases, change the reaction mechanism from a two-electron (2e) reduction to a four-electron (4e) reduction.² Even though the potential range of O₂ reduction on these surfaces might not be attractive for fuel-cell applications, an understanding of the relationship between the adlayer structure and surface catalytic activity and the origin of the adlayer catalytic action can provide guidance for designing new O₂ reduction electrocatalysts.

It is now possible to relate traditional electrochemical studies of oxygen reduction with in situ structural characteristics obtained from surface X-ray scattering (SXS) and atomic force microscopy (AFM) techniques. For instance, the reduction kinetics of O₂³ and H₂O₂^{4,5} have been related to specific atomic-level features of the surface. The present study of oxygen reduction on Bi adlayers is closely related to previous studies on Tl adlayers. The close-packed rotated-hexagonal Tl adlayer, which forms on the Au(111) surface as determined from SXS studies, supports the 2e reduction of O₂. However, it was noted that the in-plane diffraction intensity from the Tl adlayer decreased considerably with decreasing potential, suggesting a possible increased level of disorder with decreasing potential.³ At higher potentials, where the Tl rotated-hexagonal phase vanished, electrochemical measurements suggested that the 4e

oxygen reduction occurred in the potential region where the formation of an aligned incommensurate hexagonal phase occurred in alkaline solutions (SXS) and patches of the (2 × 2) phase formed in acid solutions (STM).⁶ However, in acid solutions, no ordered, low-coverage Tl phases were observed in the X-ray scattering measurements. On the basis of the present study, where the role of the cell geometry on the phase behavior was explored, we suspect that the absence of the ordered Tl phases during the course of the reaction was due to a potential shift between the sides and center of the crystal that occurred in the thin-layer geometry. This potential drop originated from the combined effects of the sheet resistance of the thin electrolyte layer (10–20 μm) and the high current from the oxygen reduction conditions.

We have carried out a comprehensive X-ray scattering study of the structural phase behavior of Bi UPD adlayers on the Au(111) surface during O₂ reduction. The “drop X-ray cell” used in the present study eliminated the complications of nonuniform current distributions inherent in conventional thin-layer X-ray cells. Both the low-coverage (2 × 2)-Bi and close-packed ($p \times \sqrt{3}$)-2Bi phases were found to be stable under O₂ reduction conditions. Here, we report a direct comparison of the structural behavior of Bi adlayers and their catalytic properties, determined from rotating disk electrode measurements, as a function of the applied potential.

2. Experimental Section

A Au(111) single crystal, 10 mm in diameter and 3 mm thick, was oriented to better than 0.1° and electropolished. The crystal surface was prepared by flame annealing immediately prior to each electrochemical or SXS measurement. After annealing, the crystal was protected by a drop of water and transferred to an electrochemical cell. The reference electrode was Ag/AgCl (3 M NaCl), and the counter electrode was a Au wire. Solutions were prepared from reagent-grade Bi₂O₃ (Aldrich), ultrapure HClO₄, and purified water (Millipore).

Two electrochemical cells were used in the in situ SXS measurements. A thin-layer cell, which utilized a thin electrolyte

* Author to whom correspondence should be addressed.

† Department of Physics.

‡ Materials Science Department.

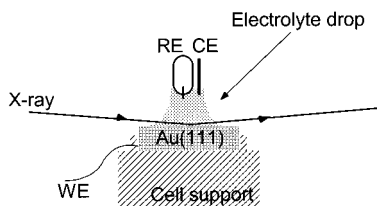


Figure 1. Schematic cross-sectional view of a drop cell for X-ray diffraction/electrochemical measurements.

solution layer (10–20 μm thick) sandwiched between the front crystal face and a thin plastic film, is described in a previous publication.⁷ The X-ray path length through the electrolyte, for a grazing incident angle of 1.25° , was approximately 1–2 mm. Whereas the thin-layer electrolyte minimized the X-ray path length through the electrolyte, a large IR voltage drop was generated between the edge and center of the crystal under reaction conditions.

For the present studies, carried out during the course of electrocatalytic reactions, we primarily utilized the “drop-cell” geometry. In the drop geometry, the counter and reference electrodes are placed directly above the crystal, within 1–2 mm of the crystal surface, to minimize the IR potential drop. The concept behind this design is similar to that behind the transmission cells used by You and Nagy,⁸ Armstrong and co-workers,⁹ Robinson and O’Grady,¹⁰ and Brossard and co-workers¹¹ where the X-ray path length is determined by the width of the solution layer rather than by its thickness. In this geometry, the diffracted signal-to-background ratio is relatively independent of the drop size as long as the wavelength-dependent X-ray penetration length through water is greater than the length of the drop. This is clearly the case at 32 keV, where the absorption length is about 35 mm. At 10 keV, where the absorption length through water is only 2 mm, the diffracted signal-to-diffuse background ratio is reduced compared to that at higher energy. However, 10 keV is ideal for studies in the thin-layer geometry. In the drop cell, shown in Figure 1, an electrolyte drop about 4 mm in diameter is confined between the Au(111) crystal at the bottom and the reference and counter electrodes at the top by capillary forces. The drop is stable for both horizontal and vertical orientations of the crystal. The Au(111) crystal, electrolyte drop, and ancillary electrodes are surrounded by an outer chamber, which permits control of the environment around the drop. Nitrogen or oxygen gas, saturated with water vapor, is slowly circulated through the outer chamber. In the case of the thin-layer cell, oxygen and nitrogen are also circulated through an outer chamber, and these gases easily permeate the thin plastic membrane that contains the electrolyte.

X-ray measurements were carried out at either 10 keV (1.197 \AA) or 32 keV (0.386 \AA) at X22A at the National Synchrotron Light Source using a vertical-scanning, four-circle diffractometer. Whereas the X-ray intensity at 32 keV was about 100 times less than that at 10 keV, the reduced absorption at 32 keV offset the loss in signal. Further, the reduced absorption also minimized the effects of X-ray-induced changes to the electrolyte. The drop-cell geometry also permitted simultaneous voltammetry measurements during the course of the X-ray measurements on the crystal face of interest.

For Au(111), reciprocal spacing is conveniently described by a hexagonal coordinate system in which $\mathbf{Q} = (a^*, b^*, c^*) \cdot (H, K, L)$, where $a^* = b^* = 4\pi/\sqrt{3}a = 2.25 \text{ \AA}^{-1}$, $c^* = 2\pi/\sqrt{6}a = 0.89 \text{ \AA}^{-1}$, and $a = 2.884 \text{ \AA}$. The in-plane diffraction measurements were carried out in the (H, K) plane with $L = 0.2$. The scattered X-ray intensities, analyzed with a 0.055° fwhm Soller

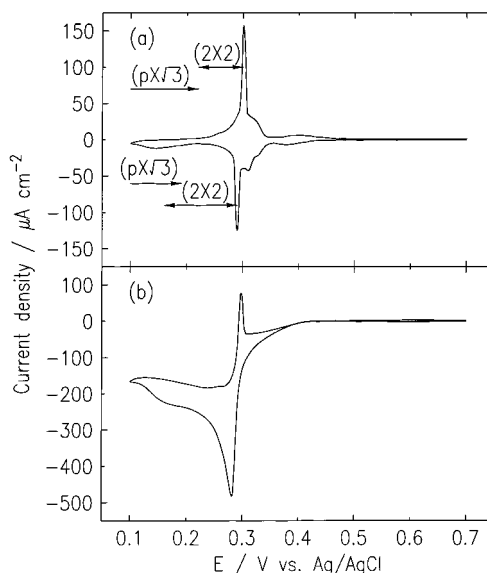


Figure 2. Voltammetry curves for (a) the UPD of Bi on a Au(111) electrode in 1 M HClO₄ with 5 mM Bi³⁺ and (b) oxygen reduction on a Au(111) surface with Bi adlayers in the same solution. Sweep rate = 10 mV s⁻¹.

slit within the scattering plane, were measured using a NaI detector. The phase behavior was determined either by using reciprocal-space scans at closely spaced potentials or by measuring the diffracted intensity versus potential at a constant (peak) position in reciprocal space. We note that the integrated intensity, a more accurate measure of the “order parameter”, differs from the peak intensity when the shape (width) of the diffraction profile changes with potential. Because the peak intensities are much easier to collect, and because the peak widths change little with potential, the peak intensities provide a sufficiently accurate measure of the phase behavior.

3. Results and Discussions

3.1. Voltammetry and Rotating Disk Electrode Studies.

Figure 2 shows typical voltammetry curves for Au(111) in 1 M HClO₄ solution containing 5 mM Bi³⁺ both (a) without and (b) with O₂. In the absence of O₂, the curves in the cathodic and anodic scans are approximately symmetrical, with three distinct regions of the Bi UPD. The number and distribution of soluble Bi species is highly dependent on the solution pH,¹² which affects the UPD process and the shape of the voltammetry curves. For the present measurements, we used 1 M HClO₄ to reduce the concentration of Bi³⁺ ions in complex forms. At about 0.4 V, a broad predeposition peak is observed, followed by a large shoulder with a superimposed sharp peak at 0.285 V and a small additional deposition associated with a weak peak at 0.15 V. Previous X-ray diffraction studies,¹³ along with the present work (vide infra), identified three phases in the Bi UPD region: a disordered adlayer; the (2 × 2)-Bi commensurate adlayer; and the incommensurate, close-packed ($p \times \sqrt{3}$)-2Bi adlayer.

The voltammetry curve in the presence of O₂ (Figure 2b) shows a large cathodic current superimposed on the characteristic Bi UPD pattern. This large cathodic current is due to O₂ reduction, which is catalyzed by the Bi adlayers. In the cathodic scan, the onset of O₂ reduction coincides with the initial adsorption of Bi. The sharp cathodic current peak at around 0.29 V is more than 3 times larger in current than the Bi UPD peak current in the absence of oxygen. This is due to the

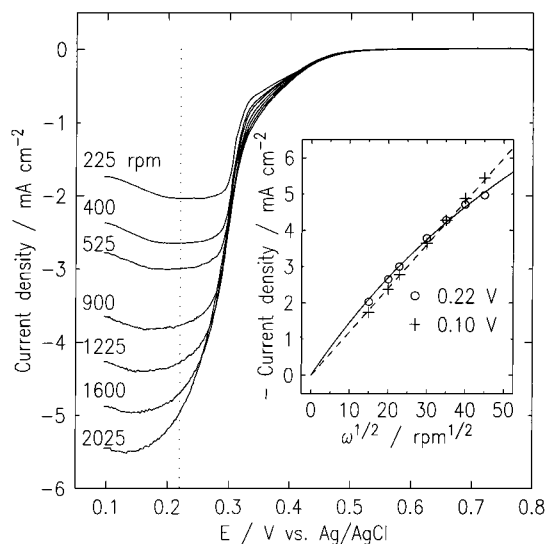


Figure 3. Rotating disk electrode measurements (anodic sweep) of O_2 reduction on a Au(111) surface with Bi adlayers in 1 M HClO_4 with 5 mM Bi^{3+} . Sweep rate = 10 mV s^{-1} . The inset shows the variation of the current density with $\omega^{1/2}$ at 0.10 and 0.22 V. Best fits are shown by the dashed and solid lines using eq 2 with $n = 3$ and eq 5 with $n = 4$ and $j_K = 17 \text{ mA cm}^{-2}$, respectively.

additional O_2 reduction current, indicating a large enhancement of the catalytic activity upon formation of the (2×2) -Bi adlayer. It is well-known that Bi adatoms have a considerable catalytic effect on O_2 reduction on Au,¹⁴ particularly in alkaline solutions.¹⁵ The half-wave potential for O_2 reduction on a bare Au(111) surface in perchloric acid solutions is ca. -0.05 V , i.e., the reaction occurs at a potential approximately 0.35 V more negative than that on the Au(111) surface with Bi adlayers.

Rotating disk electrode measurements of O_2 reduction on Au(111) with Bi adlayers are shown in Figure 3. The currents are not significantly affected by the superimposed UPD current as they are much smaller than the O_2 reduction currents under enhanced mass transport at the rotating disk electrode. Analysis of the current as a function of the rotation speed was carried out for the data at 0.10 and 0.22 V, where the $(p \times \sqrt{3})$ -2Bi and (2×2) -Bi phases, respectively, exist.

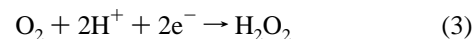
As shown in the inset in Figure 3, the linearity of the $j-\omega^{1/2}$ plot for 0.1 V indicates diffusion-controlled behavior at this potential, which can be analyzed using Levich's equation¹⁶

$$j_D = 0.62nFD_0^{2/3}\omega^{1/2}\nu^{-1/6}C_0 \quad (1)$$

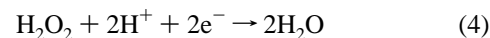
where j_D is the diffusion-limited current density, n is the number of electrons exchanged in the O_2 reduction, F is the Faraday constant, D_0 is the O_2 diffusion coefficient, ω is the rotation rate, ν is the kinematic viscosity, and C_0 is the bulk concentration of O_2 . Using the literature data for O_2 solubility ($1.38 \times 10^{-6} \text{ mol cm}^{-3}$), the diffusion coefficient ($1.9 \times 10^{-5} \text{ cm}^2 \text{ s}^{-1}$), and the kinematic viscosity ($9.97 \times 10^{-5} \text{ cm}^2 \text{ s}^{-1}$),¹⁷ eq 1 can be rewritten for oxygen reduction as

$$j_D = 0.04n\omega^{1/2} \quad (2)$$

Fitting the data at 0.1 V to eq 2 yields $n = 3.0 \pm 0.1$. In alkaline solution, it has been shown that metal adatoms (Tl, Pb, and Bi) induce a four-electron reduction reaction, which involves a two-electron exchange of O_2 to hydrogen peroxide, followed by the exchange of another two electrons to OH^- .² In acid solution, the two series reactions are



and



In this case, the measured value of $n = 3.0 \pm 0.1$ suggests that a complete 4e reduction occurs on only part of the surface. One possible scenario is that only three-quarters of the area is active for the 4e reduction process, with the remaining area being completely inactive. Alternatively, half of the area might be active to a 4e process, with the other half active only to the 2e process. Intermediate scenarios are also possible.

Despite the lower overpotential, the cathodic currents at 0.22 V, for low rotating rates, are larger than those at 0.1 V (Figure 3). The former result indicates that more active sites are available for a 4e reduction process at 0.22 V than at 0.1 V. The latter shows that the currents are partially kinetics-limited at the higher rotating rates used in the measurements. For electrode processes with slow kinetics, the current density can be expressed as

$$j = j_K/(1 + j_K/j_D) = j_K/(1 + j_K/0.04n\omega^{1/2}) \quad (5)$$

The solid line in the inset to Figure 3 shows the best fit to this form. Two parameters, j_K , the kinetics-limited current, and n were allowed to vary in the fitting, resulting in $j_K = 17 \text{ mA cm}^{-2}$ and $n = 4.0 \pm 0.2$. Note that eq 5 reduces to $j = j_D$ when $j_K \gg j_D$, which is the case for the data at 0.1 V, implying that the kinetic current is much higher at 0.10 V than at 0.22 V. This is not surprising as the reaction kinetics increase with increasing overpotential. It is interesting, however, that the number of active sites for 4e oxygen reduction is highest at intermediate potentials, where the low-coverage Bi adlayer forms, than at the most negative potential, where a close-packed Bi adlayer forms.

3.2. Surface X-ray Diffraction. As previously reported,¹³ the Bi adlayer structure can be determined by the X-ray diffraction pattern in reciprocal space. For the (2×2) -Bi adlayer, additional X-ray diffraction peaks are observed at half-order diffraction positions, e.g., $(m/2, n/2, L)$, where m and n are integers. For the $(p \times \sqrt{3})$ -2Bi phase, peaks are observed at $(-m/2 + n\delta/2, m/2 + n\delta/2)$, where δ is a measure of the incommensurability and the peaks are strongest when the sum of the integers, $m + n$, is even. Note that the incommensurate unit cell dimension is given by $p = (2\delta)^{-1}$ and the coverage is equal to 2δ . In the present study, we measured the potential-dependent X-ray scattered intensity at low-order in-plane positions and along the specular axis, both with and without oxygen, to ascertain the phase behavior of the Bi phases.

3.2.1. Bi Adlayers in the Absence of Oxygen. In the absence of large oxygen reduction currents, X-ray measurements carried out using either the thin-layer cell or the drop cell show the same structural phase behavior as a function of potential. Because the signal-to-background ratio is significantly higher in the thin-layer cell than in the drop cell, the former is preferred when the IR drop is not a limiting factor, especially for measuring weak diffraction peaks. The results for 1 M HClO_4 solution obtained in this study are similar to those found for 0.1 M HClO_4 solution reported earlier.¹³

Figure 4a shows the real-space models of the (2×2) -Bi adlayer. Because the area of this primary unit cell is 4 times of that of the substrate, the Bi coverage relative to the atomic density of the Au(111) substrate is 0.25. The more densely packed $(p \times \sqrt{3})$ -2Bi phase (see Figure 4b) has a rectangular unit cell, with one atom slightly displaced from the centered

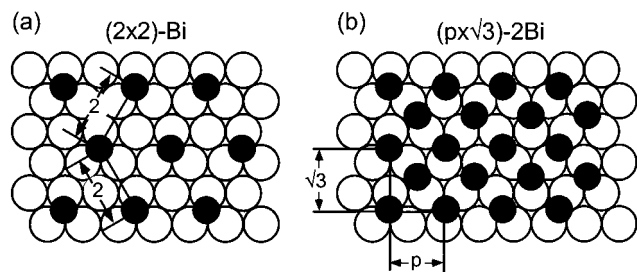


Figure 4. Real-space models for the (a) (2×2) -Bi and (b) $(p \times \sqrt{3})$ -2Bi adlayers on Au(111) resulting from the UPD of Bi from solution as in Figure 2.

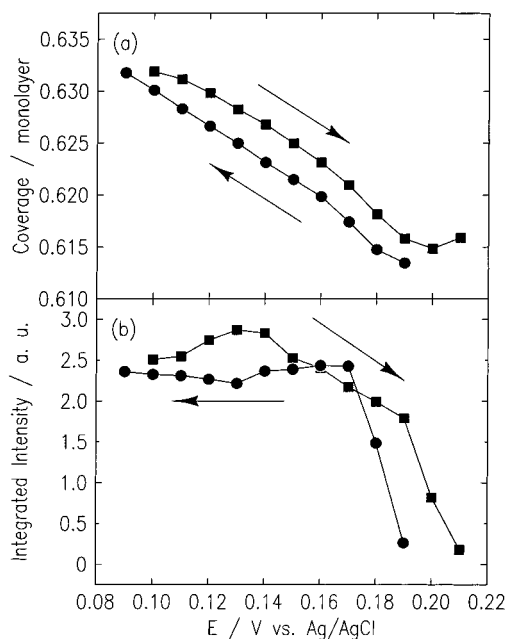


Figure 5. Bi coverages calculated from (a) the measured peak position and (b) the integrated intensity for the $(p \times \sqrt{3})$ -2Bi phase as a function of potential in the absence of O_2 for two sweep directions obtained in a thin-layer cell.

position along the commensurate $\sqrt{3}$ direction. The potential-dependent Bi coverage in this uniaxially incommensurate phase was obtained by measuring potential-dependent peak positions from the Bi adlayer. As shown in Figure 5a, the coverage varies linearly with potential and increases from 0.613 at 0.19 V to 0.632 at 0.09 V. Further, there is hysteresis between the two sweep directions. The coverage is close to the value of 0.55 obtained from integrating the charge in the voltammetry curve. Figure 5b also shows the integrated scattering intensity as a function of potential. The rapid increase in the intensity at 0.19 V results from the first-order phase transition from the (2×2) -Bi to the $(p \times \sqrt{3})$ -2Bi phase.

3.2.2 The (2×2) -Bi Phase on Au(111) during Oxygen Reduction. Figure 6 shows the potential dependence of the scattered intensity (peak intensity) at $(\frac{1}{2}, \frac{1}{2}, 0.2)$ in the presence of O_2 or N_2 gas in the outer chamber and, hence, with or without a large oxygen reduction current. This intensity at this reciprocal-space position is a direct measure of the presence of the (2×2) -Bi phase. We note that the intensities are slightly larger in the positive potential sweep than in the negative sweep. Although the scattered intensities are the same for O_2 and N_2 in the positive sweep, in the negative sweep, the data are slightly higher for the oxygen-saturated electrolyte. These differences might originate from the fraction of the surface covered with the (2×2) -Bi phase or from slight changes in the diffraction

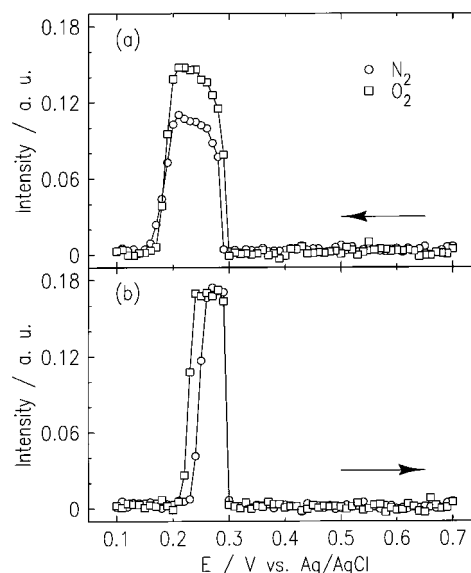


Figure 6. X-ray scattered intensity at the $(\frac{1}{2}, \frac{1}{2}, 0.2)$ position as a function of potential in the presence of either O_2 or N_2 (no oxygen) obtained in a drop cell. $\lambda = 0.386 \text{ \AA}$; sweep rate = 2 mV s^{-1} ; solution composition as in Figure 2. The differences in the peak intensities for O_2 and N_2 might result from small differences in the relative coverage or diffraction width.

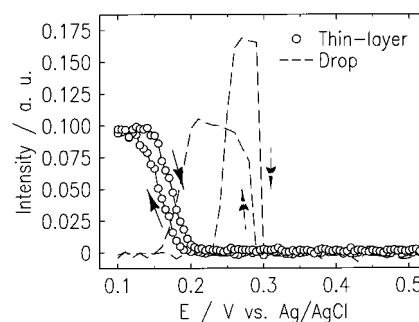


Figure 7. X-ray scattered intensity at the $(\frac{1}{2}, \frac{1}{2}, 0.2)$ position as a function of potential in the presence of O_2 obtained in thin-layer and drop cells. $\lambda = 0.386 \text{ \AA}$; sweep rate = 2 mV s^{-1} ; solution composition as in Figure 2.

widths. In either case, these differences do not alter our ability to identify the phase transitions. Our results, obtained in the drop cell, clearly show that the formation and disappearance of the (2×2) -Bi phase are practically unaffected by O_2 reduction. The transition potential between the (2×2) -Bi phase and the disordered Bi phase occurs at 0.3 V, independent of the sweep direction. On the other hand, the transition potential between the (2×2) -Bi phase and $(p \times \sqrt{3})$ -2Bi phase depends strongly on the sweep direction.

We also compared the potential dependence of the (2×2) -Bi phase for the two electrochemical cells. In Figure 7, we show the scattered intensity (peak intensity) at $(\frac{1}{2}, \frac{1}{2}, 0.2)$ in the presence of O_2 in the drop and thin-layer cells for the same solution. The phase transition potentials are shifted negatively by about 0.1 V relative to those obtained in the drop cell. This can be attributed to the IR voltage drop across the crystal surface. When the current is cathodic, an IR voltage drop causes a positive potential offset; therefore, the phase transitions are observed at more negative potentials. In addition, the potential region of the phase transition is broadened because of the uneven IR potential drop over the sampling area. These results demonstrate the importance of the cell geometry for in situ structural studies under reaction conditions.

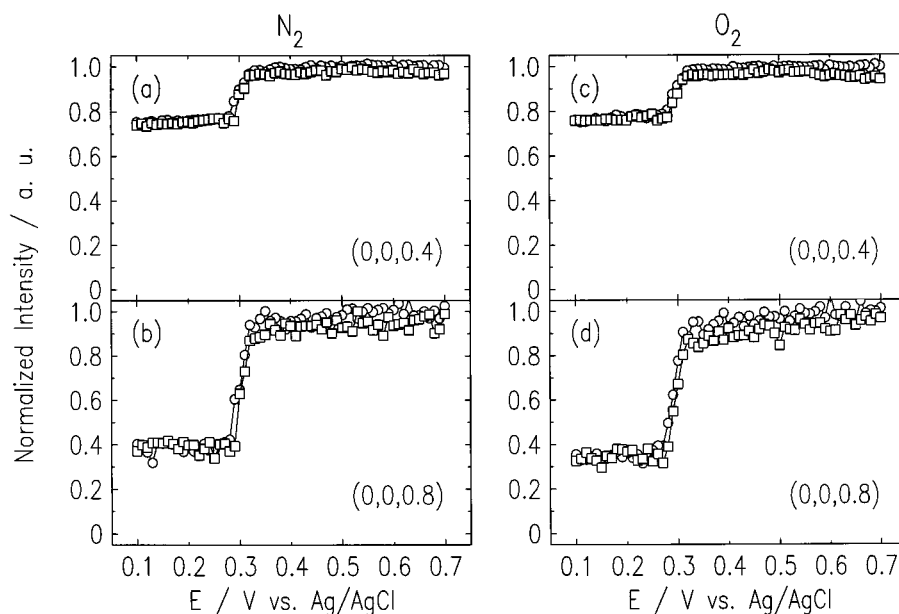


Figure 8. Normalized scattered intensity as a function of potential at two positions along the specular reflectivity rod (a and b) in the absence of O_2 and (c and d) in the presence of O_2 obtained in a drop cell. Squares and circles are for the anodic and cathodic scans, respectively; sweep rate = 2 mV s^{-1} .

The X-ray scattered intensity at specular positions is sensitive to the surface normal structure, e.g., layer coverage, layer spacing, and surface roughness, and is not sensitive to the lateral surface structure of the adlayer. At small values of L , where Debye–Waller roughness effects are small, the potential-dependent reflectivities provide a rather direct measure of the bismuth coverage in the limit that the layer spacing is independent of coverage. This coverage information complements that provided by the in-plane structure measurements. An exact expression for this dependence can be obtained by considering the relative scattering amplitudes from the Au and Bi atoms in this case.

In Figure 8, we show the scattered intensities versus potential at $(0, 0, 0.4)$ and $(0, 0, 0.8)$ obtained in the drop cell. No changes in the scattering widths were observed with potential. In both sweep directions, the scattered intensity undergoes a sharp change at around 0.3 V. This change is clearly correlated with the sharp current peaks observed in the voltammetry curve (Figure 1). Neither the phase transition potential nor the intensities at potentials below 0.3 V are affected by the presence of oxygen. These observations further confirm the stability of the Bi adlayer during the course of oxygen reduction.

It can be seen, however, that there is no change corresponding to the phase transition between the two ordered phases in Figure 8, despite their significantly different coverages. Calculations of the reflectivity at the above two positions, using a semi-infinite sum over the atomic layers, were made for both the (2×2) Bi adlayer with 0.25 monolayer coverage and the $(p \times \sqrt{3})$ phase with an average coverage of 0.63 monolayer. The results are listed in Table 1, together with the measured values. The good agreement between the calculated and measured values support the structure model derived from the in-plane diffraction study. Despite the small change in reflectivity for these two coverages, this is a peculiarity of the coverages of the ordered phases. For instance, at coverages close to 0.5, much larger changes in the reflectivity would be expected. The model also predicts a small difference in the value of the reflectivity for the two different ordered phases, despite the very large difference in coverage, and supports our finding that this transition is not readily identifiable in the data.

TABLE 1: Values of Reflectivity (%) Obtained by Experiments and Calculations

coverage (monolayer)	L^a	experimental		calculation
		N_2	O_2	
0.25	0.4	77	79	81
	0.8	36	36	42
0.63	0.4	75	76	78
	0.8	40	36	37

^a In units of c^* .

3.2.3. The $(p \times \sqrt{3})$ -2Bi Phase on Au(111) during Oxygen Reduction. To address the issue of whether the $(p \times \sqrt{3})$ -2Bi phase is stable during oxygen reduction, we carried out additional measurements in both the drop and thin-layer cells. In the drop cell, these measurements are complicated by the weak scattered intensity from the incommensurate $(p \times \sqrt{3})$ -2Bi phase compared to the diffuse scattered intensity. As a result, it is difficult to acquire an accurate measure of the incommensurability in this geometry. However, the presence of the $(p \times \sqrt{3})$ -2Bi phase could be verified by the scattered intensity at $(0, \frac{1}{2}, 0.2)$, which is nonzero in both the $(p \times \sqrt{3})$ -2Bi and (2×2) -Bi phases, although it is a factor of 4 times weaker in the former phase. The potential dependence at this position (not shown) clearly indicates that the $(p \times \sqrt{3})$ -2Bi phase is virtually unaffected by the presence of the oxygen reduction current.

An additional measure of the structure of the $(p \times \sqrt{3})$ -2Bi phase during the course of oxygen reduction can be obtained by measuring the incommensurate wave vector as a function of potential in the thin-layer geometry. For these measurements, oxygen gas is circulated in the outer chamber of the cell. To minimize the current-induced potential shift, the X-ray beam is displaced from the center of the cell. The diffraction peak from the $(p \times \sqrt{3})$ -2Bi phase is observed over nearly the same 100-mV potential region as in the absence of O_2 . The Bi coverage, determined from the measured reciprocal-space peak position as a function of potential, shown in Figure 9, is slightly decreased in the presence of oxygen. This apparent coverage decrease is attributed to a positive potential offset due to the IR drop in the thin-layer cell and not to affect of oxygen

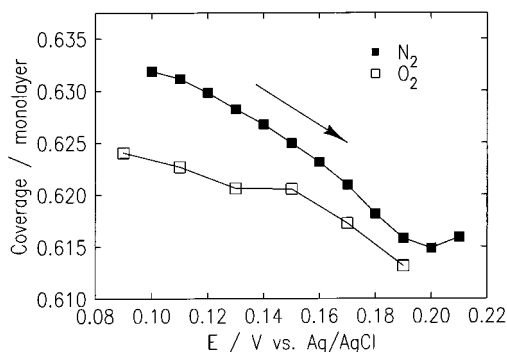


Figure 9. Bi coverage calculated from the measured peak position for the $(p \times \sqrt{3})$ -2Bi phase as a function of potential using a thin-layer cell in the presence and in the absence of O_2 . $\lambda = 0.386 \text{ \AA}$; solution composition as in Figure 2.

reduction. This finding supports our measurements in the drop-cell geometry, which also indicated that the O_2 reduction does not affect the presence and structure of the Bi $(p \times \sqrt{3})$ -2Bi phase.

3.3. Origin of the Catalytic Action of Bi Adlayers. The implications of these findings for electrocatalysis and catalysis, and in particular for O_2 reduction electrocatalysis, are noteworthy. They show that, even under oxidizing conditions, sub-monolayers of nonnoble metals can form stable structures. The Bi adatoms, which are active sites for O_2 reduction, do not leave the Au surface where they reside. How do O_2 molecules interact with the bismuth-coated gold surface to give rise to the enhanced catalytic activity? Is the interaction solely with the surface Bi adatoms, or is it with both gold and bismuth atoms through the formation of a bridge bond? Gewirth and co-workers⁵ proposed that the latter mechanism facilitates O–O bond scission.⁶ Alternatively, Sayed and Jüttner¹⁴ proposed that the UPD Bi accelerates the rate-determining first electron-transfer step, $O_2 + e^- \rightarrow O_2^-(ads)$, through a stronger adsorption of the O_2^- superoxide radical. We believe that a large shift of the reaction to more positive potentials, in comparison with the reaction on bare Au, requires an increase in the energy of O_2 adsorption, which is likely to be provided by the Bi adatoms. On the other hand, the less active sites for 4e reduction on the close-packed $(p \times \sqrt{3})$ -2Bi adlayer compared to the open structure of the (2×2) -Bi phase seem to support the mechanism involving the formation of a bridge bond between O_2 and Au and Bi adatom sites, provided that there is no change in the state of the Bi adatoms at the more negative potentials corresponding to the existence of the incommensurate phase.

4. Conclusions

Structures of Bi UPD adlayers on Au(111) have been studied during catalytic O_2 reduction by surface X-ray scattering

techniques using both electrochemical drop and thin-layer cells. These measurements are complemented by electrochemical measurements, including those with a rotating disk electrode. These results indicate that the stability and phase transition behavior of the (2×2) -Bi and $(p \times \sqrt{3})$ -2Bi phases are not significantly affected by O_2 reduction. These data are the first direct observation of an active adlayer phase that is not affected by an electrocatalytic reaction. Oxygen reduction at Au(111) with the (2×2) -Bi adlayer is shifted by 0.35 V to more positive potentials and proceeds with an exchange of four electrons, albeit with relatively slow kinetics. The close-packed $(p \times \sqrt{3})$ -2Bi phase, formed at more negative potentials, appears to have limited sites available for the four-electron reduction but to result in enhanced reaction kinetics as a result of the increased overpotential.

Acknowledgment. This work was supported by the U.S. Department of Energy, Divisions of Chemical and Materials Science, under Contract DE-AC0298CH10886. K. Tamura acknowledges the Japan Society for the Promotion of Science for fellowships to do research abroad during the years 2000–2002.

References and Notes

- (1) Gottesfeld, S.; Zawodzinski, T. A. In *Advances in Electrochemical Science and Engineering*; Alkire, R. C., Kolb, D. M., Eds.; Wiley-VCH: Weinheim, Germany, 1997; Vol. 5, Chapter 4.
- (2) Adžić, R. R. *Advances in Electrochemistry and Electrochemical Engineering*; Gerischer, H., Tobias, C., Eds.; Wiley: New York, 1984; Vol. 13, pp 159–260.
- (3) Adžić, R. R.; Wang, J. X.; Ocko, B. M. *Electrochim. Acta* **1995**, *40*, 83.
- (4) Chen, C.-h.; Gewirth, A. A. *J. Am. Chem. Soc.* **1992**, *114*, 5439.
- (5) Oh, I.; Biggin, M. E.; Gewirth, A. A. *Langmuir* **2000**, *16*, 1397.
- (6) Adžić, R. R.; Wang, J. X. In *Oxygen Electrochemistry*; Adžić, R. R., Anson, F. C., Kinoshita, K., Eds.; The Electrochemical Society: Pennington, NJ, 1996; Vol. 95-26, p 61.
- (7) Wang, J.; Ocko, B. M.; Davenport, A.; Isaacs, H. *Phys. Rev. B* **1992**, *46*, 10321.
- (8) Nagy, Z.; You, H.; Yonco, R. M.; Melendres, C. A.; Yun, W.; Maroni, V. A. *Electrochim. Acta* **1991**, *36*, 209.
- (9) Armstrong, M. J.; Whitney, G. M.; Toney, M. F. In *X-ray Methods in Corrosion and Interfacial Electrochemistry*; Davenport, A., Gordon, J. G., II, Eds.; The Electrochemical Society: Pennington, NJ, 1992; p 62.
- (10) Robinson, K. M.; O'Grady, W. E. *Rev. Sci. Instrum.* **1993**, *64*, 1061.
- (11) Brossard, F.; Etgens, V. H.; Tadjeddine, A. *Nucl. Instr. Methods Phys. Res. B* **1997**, *129*, 419.
- (12) Baes, F. M.; Mesmer, R. E. *Hydrolysis of Cations*; Wiley-Interscience: New York, 1976.
- (13) Chen, C.-h.; Kepler, K. D.; Gewirth, A. A.; Ocko, B. M.; Wang, J. *J. Phys. Chem.* **1993**, *97*, 7290.
- (14) Sayed, S. M.; Jüttner, K. *Electrochim. Acta* **1983**, *28*, 1635.
- (15) Adžić, R. R.; Marković, N. M.; Tripković, A. V. *Bull. Soc. Chem. Belgrade* **1980**, *45*, 399.
- (16) Levich, V. G. *The Physicochemical Hydrodynamics*; Prentice Hall: Englewood Cliffs, NJ, 1962.
- (17) Gubbins, K. E.; Walker, R. D. *J. Electrochem. Soc.* **1965**, *112*, 469.